AIAA SciTech 2015
January 5–9, 2015
Kissimmee, FL

AIAA 2015-1930

Simulation of Atmospheric-Entry Capsules in the Subsonic Regime

Scott M. Murman, Robert E. Childs,* and Joseph A. Garcia

NASA Ames Research Center, Moffett Field, CA, USA

Abstract

The accuracy of Computational Fluid Dynamics predictions of subsonic capsule aerodynamics is examined by comparison against recent NASA wind-tunnel data at high-Reynolds-number flight conditions. Several aspects of numerical and physical modeling are considered, including inviscid numerical scheme, mesh adaptation, rough-wall modeling, rotation and curvature corrections for Reynolds-averaged eddy-viscosity models, and Detached-Eddy Simulations of the unsteady wake. All of these are considered in isolation against relevant data where possible. The results indicate that an improved predictive capability is developed by considering physics-based approaches and validating the results against flight-relevant experimental data.

1 Introduction

Accurate prediction of the aerodynamic loads on atmospheric-entry capsules is still a challenge for Computational Fluid Dynamics (CFD) primarily due to the three-dimensional separation and unsteady wake flow. At high supersonic speeds the combination of high dynamic pressures and suppression of some of the wake unsteadiness makes the problem tractable, and consistent predictions with common engineering Reynolds-averaged Navier-Stokes (RANS) models is often possible. When peak dynamic pressure is passed during

*Science and Technology Corporation.

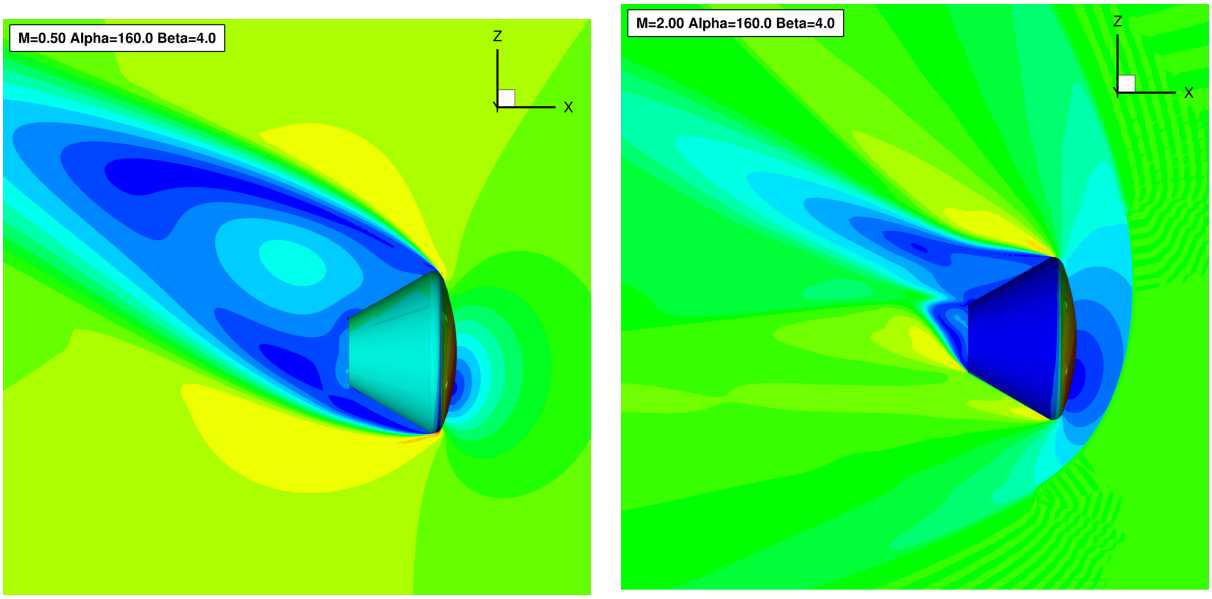

(a) Subsonic **(b)** Supersonic

Figure 1: Contours of Mach number in an Orion capsule wake at supersonic and subsonic speeds

the entry profile and the capsule enters the transonic and subsonic regimes, the unsteady wake "opens up" and errors in turbulence modeling can have a much greater impact on the prediction of aerodynamic performance (*cf.* Fig. 1). Unfortunately, this is often where greatest accuracy is required for Earth-entry systems, as there is little margin in control authority and complex parachute decelerator staging must be accomplished for targeted landing. Within NASA, the Orion Multi-Purpose Crew Vehicle project (*cf.* Fig. 2) is studying the requirements for consistent aerodynamic predictions using current "production" engineering CFD solvers and turbulence models. Simulations of the Orion vehicle for human exploration are further complicated by the existence of a rough ablated heatshield during normal mission profiles, and a smooth heatshield during abort scenarios. As will be shown, these two heatshield surfaces produce strongly differing aerodynamic environments.

While there are numerous examples of simulation predictions for the high-speed aerothermodynamic environment of a capsule entry, there are only a handful of publications in the open literature that consider subsonic flow predictions[1–4]. These studies concentrate on predicting the integrated loads for either Apollo test results[5] or data from a preliminary Orion wind tunnel experiment[6]. Unfortunately, both of these validation datasets suffer from undocumented transitional and partially tripped boundary layers on the capsule heatshield, leading to inconsistent conclusions for validation purposes.

Figure 2: Artists rendition of the Orion Multi-Purpose Crew Vehicle.

The current work details current "lessons learned" in prediction of aerodynamic loads for the Orion capsule in the subsonic regime, in comparison to recent experimental data[7–9]. These experiments were specifically designed to overcome the limitations of previous efforts and provide CFD validation data at flight Reynolds numbers in the subsonic and transonic regime. Figure 3 presents computed integrated loads against the recent experimental data at Mach 0.5, which is the flight condition that the current work will focus upon. This work utilizes the OVERFLOW solver[10], and the predictions in Fig. 3 use (heretofore) standard inputs for developing an aerodynamic database across all speed regimes, namely: roughly 30M grid points to resolve the capsule geometry and near wake, the upwind Harten-Lax-van Leer-Contact (HLLC) method for robustness and accuracy in flows with shock waves, and Menter's Shear-Stress-Transport (SST) model[11] for the Reynolds-averaged Navier-Stokes (RANS) equations. The CFD predictions are notably off in both drag and pitching moment*. Further, two of the angles of attack develop unsteady RANS flowfields, while the others remain steady. This inconsistency causes problems when using RANS methods to develop increments to augment the experimental test results, as the flows which develop unsteadiness are not known *a priori*, and are configuration dependent.

The current paper examines issues potentially leading to the mis-predictions outlined in Fig. 3, including numerical methods, mesh resolution, and turbulence modeling. These are investigated through comparisons against experimental data including integrated loads, surface pressure distributions, boundary-layer profiles, and Particle Image Velocimetry (PIV) measurements of the extended wake flowfield. A companion paper is available examining

*The pitching moment is computed about the "theoretical" apex of the capsule geometry.

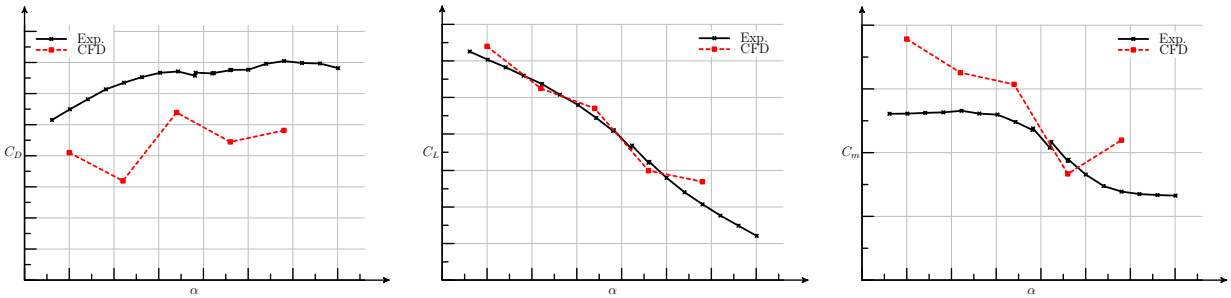

(a) Drag **(b)** Lift **(c)** Pitching Moment

Figure 3: Computed and experimental integrated loads for an Orion capsule geometry using standard methods for constructing an aerodynamic database. $M_\infty = 0.5$, $Re_D = 24$M.

similar issues using the OpenFOAM solver[12].

2 Wall Roughness

The majority of the current work uses a simplified capsule model developed for public release in the experimental program described in [9](*cf.* Fig. 4). While the capsule is a straightforward axisymmetric shape, the inclusion of the strut support adds significant geometric complication. Further, an actual atmospheric-entry capsule geometry includes cutouts, windows, reaction-control surfaces, *etc.* which make the geometry definition more complex (*cf.* Fig. 2). In order to accommodate these complex geometries, while still maintaining computational efficiency, a structured overset grid system is utilized with the OVERFLOW solver. The overset grid system corresponding to the wind tunnel configuration of Fig. 4 is shown in Fig. 5. This baseline grid system has 42M points and can be further adapted using the OVERFLOW solver[13, 14].

The AVCOAT honeycomb, which is the current Orion capsule heatshield design, ablates to a hexagonal roughness pattern. This roughness pattern scaled to the experimental capsule heatshield from [9] is shown in Fig. 6. OVERFLOW does not contain a standard wall roughness model. The roughness model of Knopp *et al.* [15] was implemented in OVERFLOW and verified using flat-plate boundary layer simulations. This model uses an equivalent sand-grain approach which does not accurately capture the boundary layer response to discrete roughness elements, as we have on the capsule heatshield. It is necessary to empirically calibrate the model for discrete roughness, which is done here using a multiplicative scale factor applied to the true roughness height. The model is calibrated at $M_\infty = 0.7$, $\alpha = 150°$ against boundary layer profiles from [9], and then this calibration is tested against other

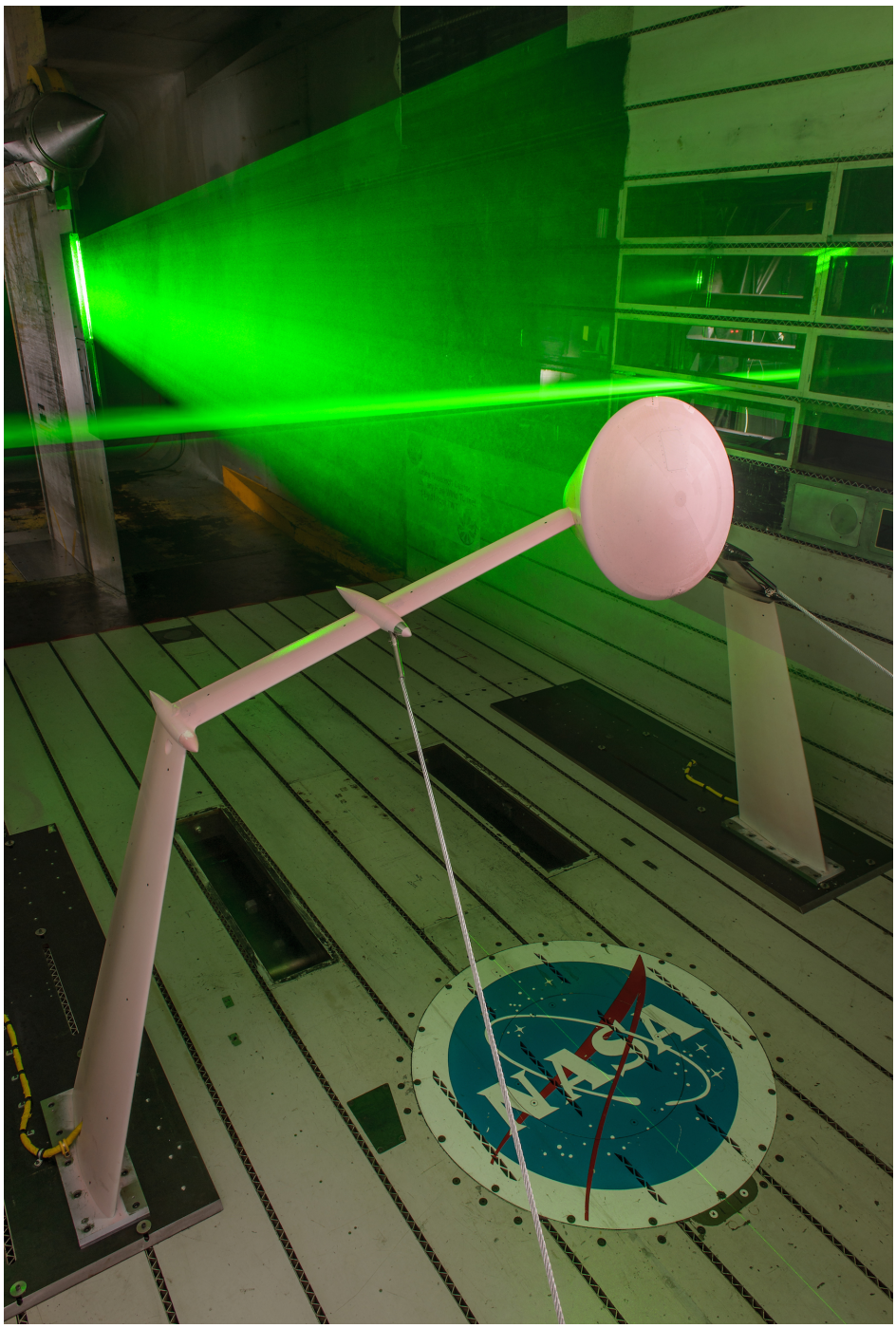

Figure 4: Capsule and strut configuration in the NASA Ames 11 ft. transonic wind tunnel[9]. The model is coated with PSP and the horizontal and vertical laser sheets cover the wake PIV planes.

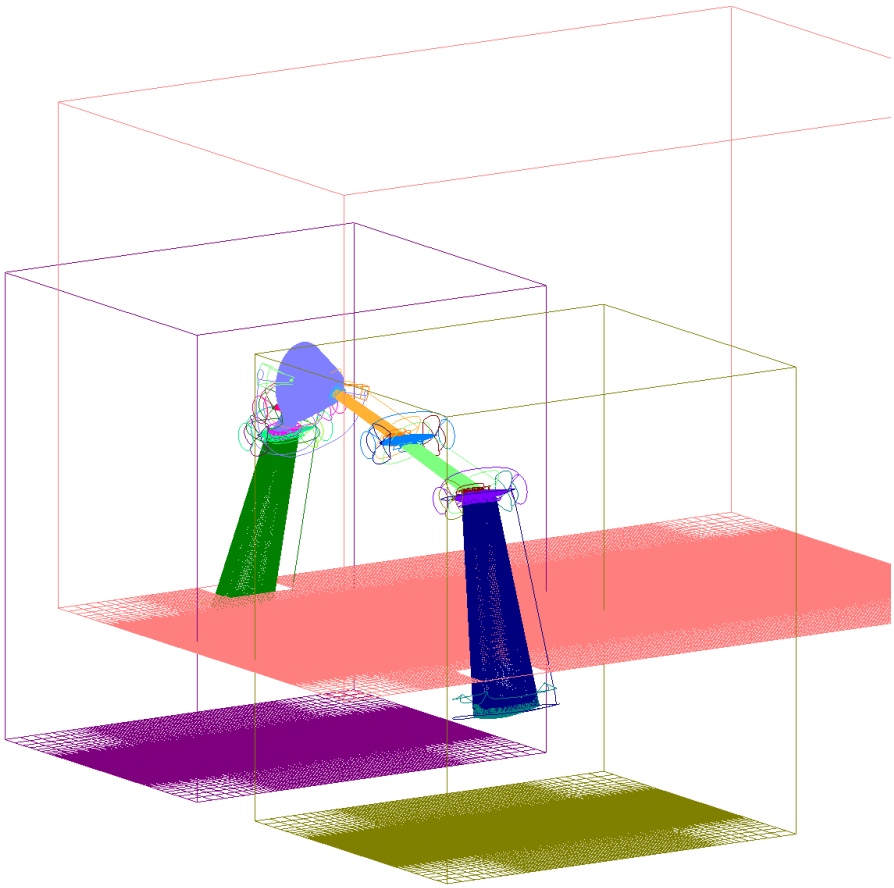

Figure 5: Overset grid system for the capsule and strut configuration in the NASA Ames 11 ft. transonic wind tunnel[9].

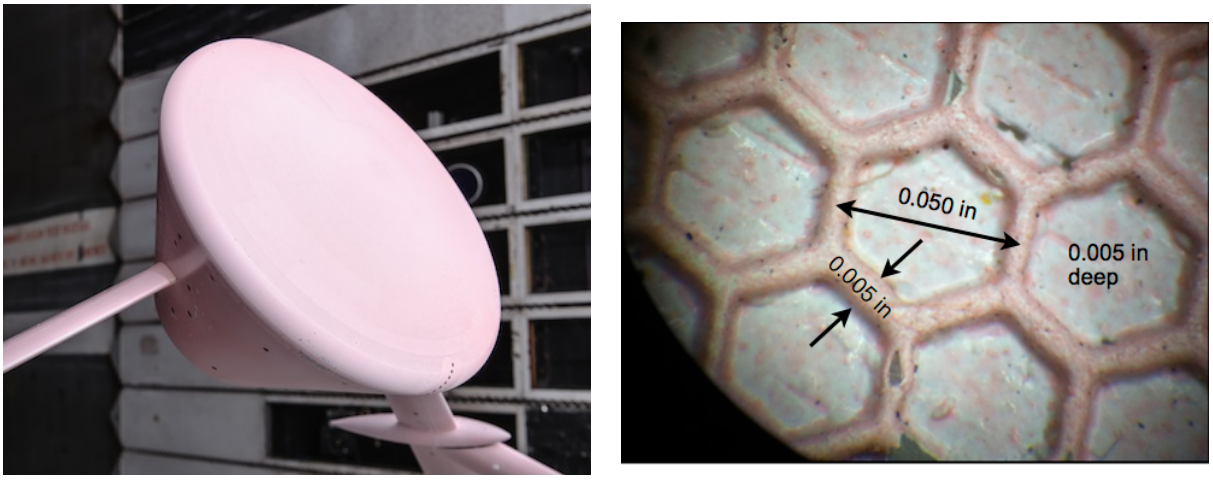

Figure 6: Hexagonal roughness from the experimental model in [9].

available experimental conditions. The probe is located on the lateral plane of symmetry, just upstream of where the windward side boundary layer separates from the heatshield. Figure 7 shows the experimental and computational boundary layer profiles on the heatshield at $M_\infty = 0.7$, $\alpha = 150°$. Discrete roughness scaling factors of $k_{SF} = 2$, 4, and 10 are tested, with a value of $k_{SF} = 4$ providing a good fit for the rough-wall profile. This value of $k_{SF} = 4$ is found to be a good fit at other flow conditions as well (Fig. 8), and all rough wall simulations presented herein use this scaling factor.

Figure 9 presents the computed surface pressure coefficient on the experimental model for a smooth and rough wall approximation. The presence of roughness reduces the "suction peak" near the heatshield shoulder associated with the attached boundary layer just upstream of separation from the surface by over 25% at these conditions. This is consistent with experimental observations, and is the motivation for including this roughness effect in the current computational approach.

3 Detached Eddy Simulations

There are three main turbulence models currently supported by OVERFLOW: the Spalart-Allmaras model[16], Wilcox's k-ω model[17], and Menter's Shear-Stress-Transport (SST) model[11]. From experience in the Orion project, the SST model has provided the most consistent predictions for capsule flowfields (*cf.* Childs *et al.* [18], Stremel *et al.* [3] for an overview of the issues), and is the baseline model utilized in this work. Given this modeling

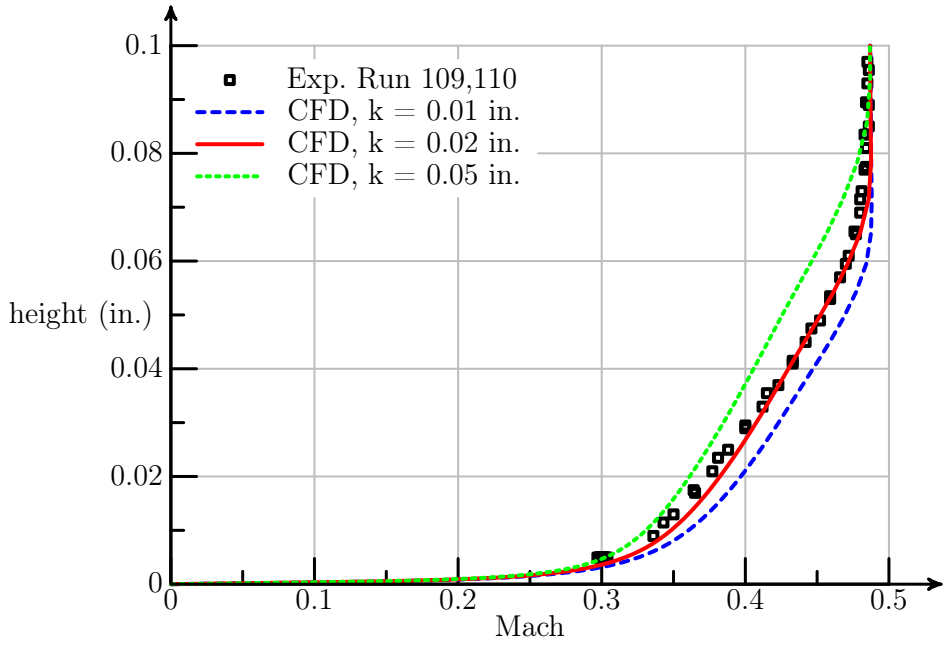

Figure 7: Calibration of the discrete roughness scale factor to the capsule heatshield boundary layer. The experimental roughness height is 0.005 in. $M_\infty = 0.7$, $\alpha = 150°$. Experimental data taken from [9].

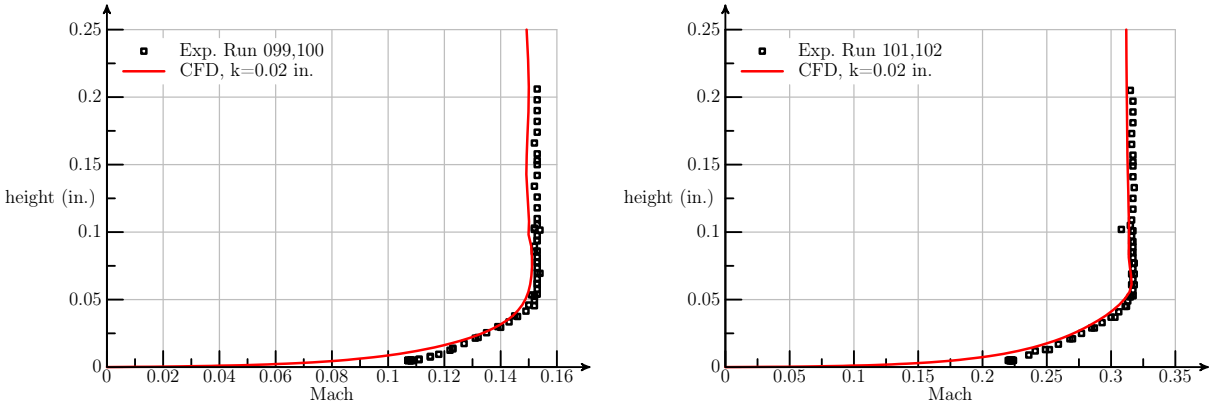

(a) $M_\infty = 0.3$, $\alpha = 166°$ **(b)** $M_\infty = 0.7$, $\alpha = 166°$

Figure 8: Test of the calibrated discrete roughness scale factor $k_{SF} = 4$. The experimental roughness height is 0.005 in. Experimental data taken from [9].

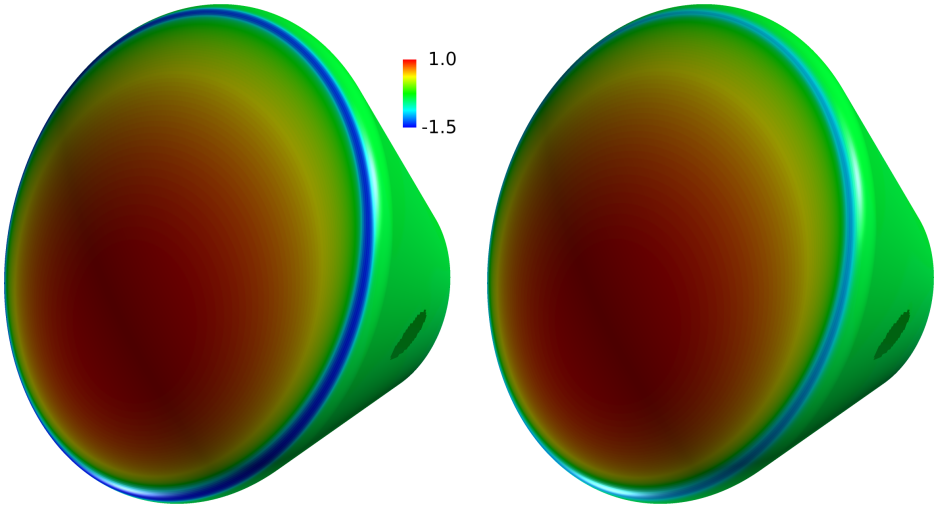

(a) smooth **(b)** rough

Figure 9: Computed distribution of surface pressure coefficient $M_\infty = 0.5$, $\alpha = 166°$, $Re_D = 8.7$M.

framework, several augmentations are available. In the current work we investigate the use of hybrid-RANS/Detached-eddy Simulations (DES) to accurately capture the unsteady wake and the rotation and curvature correction of Spalart and Shur[19] in the near-wall region. The SST-DES simulations are first considered in this section.

Simulations of the experimental configuration from [9] using RANS and DES simulations were performed using the rough wall model at $M_\infty = 0.5$, $\alpha = 166°$, $Re_D = 8.7$M. The unsteady DES simulations are time averaged after reaching a stationary state. Fig. 10 shows a typical unsteady load variation for a DES simulation after the initial transient, along with the same data as a distribution function. The data is averaged over 1 second of physical time, however this is still not sufficient to ensure statistical convergence, and hence there is still some uncertainty in the time-averaged values. The simulations use a timestep which resolves the primary vortex shedding frequency (computed using a Strouhal number of 0.2) with 50 steps per shedding cycle. The difference between the computed surface pressure and the pressure measured by the experimental pressure-sensitive paint (PSP) system is presented in Fig. 11. On the windward side of the capsule, the major discrepancy occurs near the suction peak and separation region for both simulations. The location of the experimental Kulite unsteady pressure transducers is visible from the increase in difference at the 12, 1, and 3 o'clock positions. The region surrounding the Kulite installation is smooth in the experiment, and this local change is not modeled in the computations. As expected, for the attached boundary layer on the heatshield both RANS and DES simulations are essentially

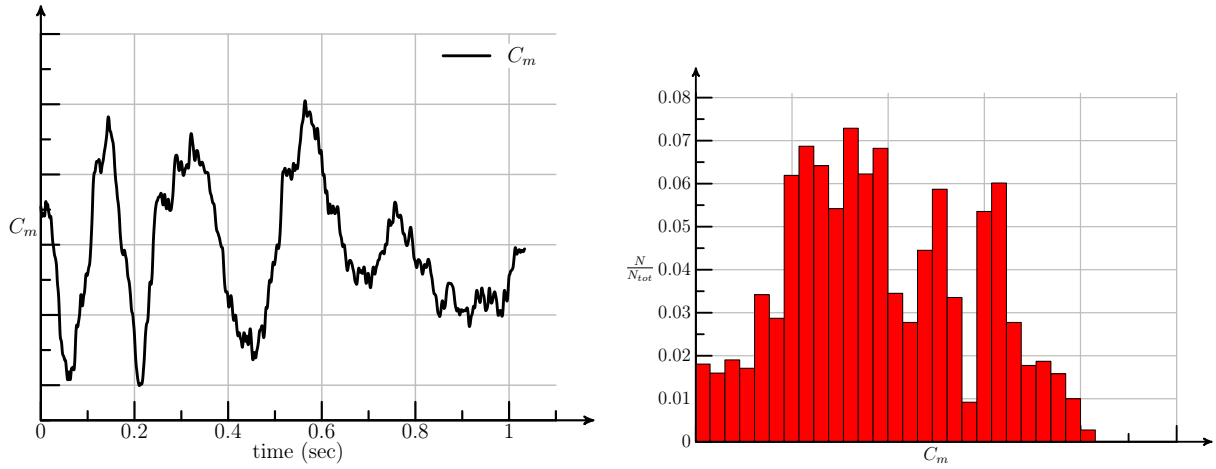

(a) Time History **(b)** Distribution

Figure 10: Unsteady variation of pitching moment for a DES simulation. The transient portion of the simulation has been removed.

	PSP	RANS	DES
C_D	0.93	0.82	0.85
C_L	0.03	0.023	0.019

Table 1: Computed aerodynamic loads. $M_\infty = 0.5$, $\alpha = 166°$, $Re_D = 8.7$M.

identical. The largest difference in the simulations occurs in the aft base region, where the RANS simulation overpredicts the pressure coefficient by roughly 30% of the freestream dynamic pressure, comparable to the magnitude of the difference near the suction peak. As we will see in the next section, the wake velocity in this region is also difficult for the RANS model to predict. The computed results consistently predict a delayed boundary-layer separation on the heatshield, and this drives the differences in the computed suction peak on the heatshield. Table 1 provides the computed lift and drag compared with the integrated PSP value. Consistent with the predictions of surface pressure, the numerical results under-predict the drag by roughly 10%.

3.1 Wake Velocity Predictions

The rough-wall RANS and DES simulations outlined in the previous section are compared to the PIV wake velocity measurements in Fig. 12. Both the computations and experimental data present time-averaged data. Qualitatively, the computations are in relatively good agreement with the measurements, with the shear layer and reversed flow wake clearly

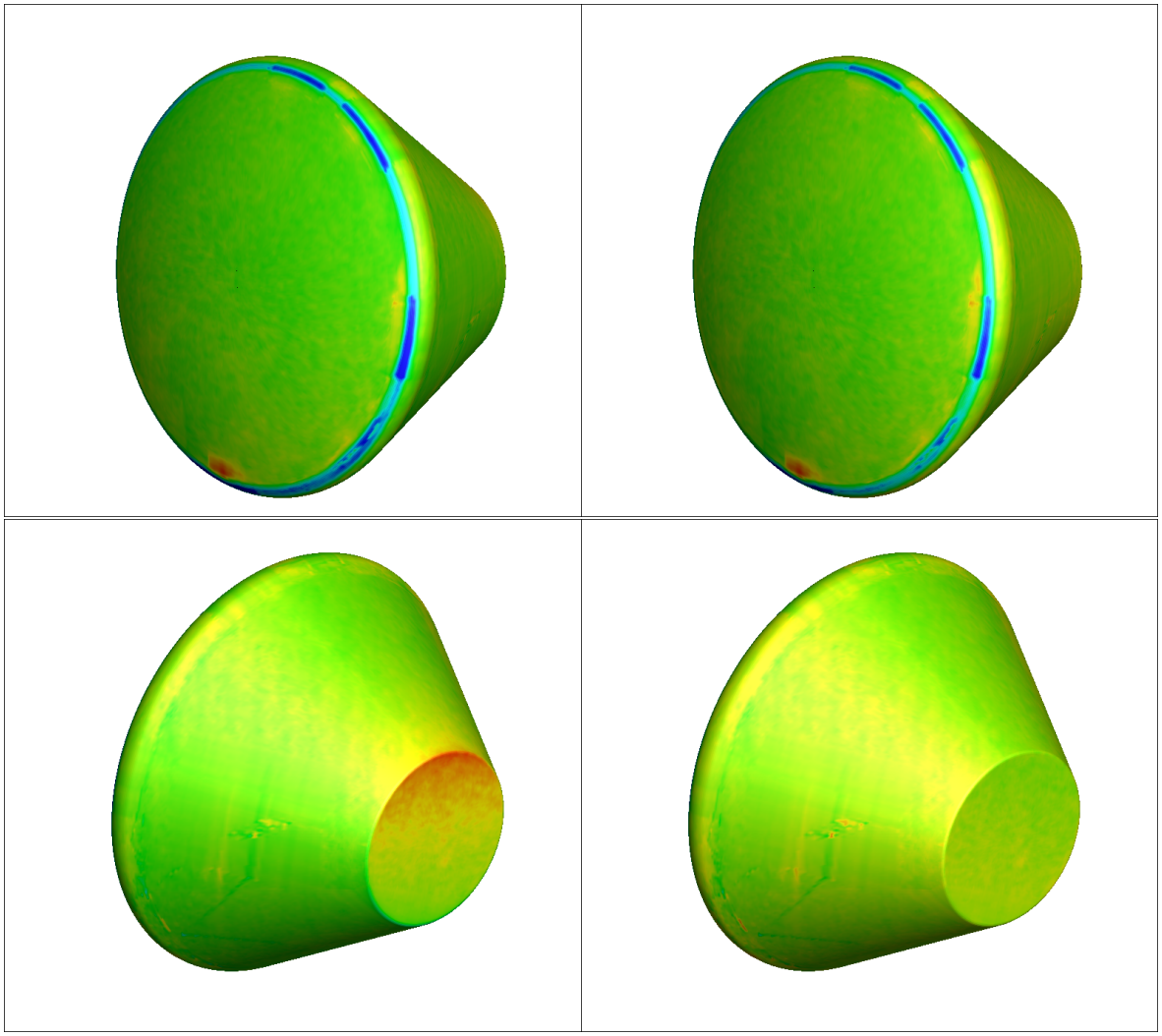

RANS DES

Figure 11: Difference in the surface pressure coefficient between simulation and PSP measurement (CFD-PSP). The limits of the difference are $\pm 0.3 q_\infty$, with green representing zero difference. $M_\infty = 0.5$, $\alpha = 166°$, $Re_D = 8.7$M.

	# Grid Pts.	RANS	DES
1x	42M	0.079	0.06
2x	47M	0.085	0.056
4x	79M	0.086	0.074

Table 2: Relative r.m.s. difference in the computed wake velocity magnitude relative to the PIV measurements. $M_\infty = 0.5$, $\alpha = 166°$, $Re_D = 8.7$M.

visible. To highlight the differences, the CFD predictions are subtracted from the PIV measurements (Fig. 13). This shows relatively large error in the RANS far wake prediction, and in the prediction of the location of the separated shear layer for both simulations. This is expected from the discrepancy in boundary layer separation location highlighted in the previous section. The RANS near wake also contains a relatively large error near the aft body of the capsule, consistent with the difference in surface pressure from Fig. 11.

An isotropic mesh refinement study was undertaken for the capsule wake region for both RANS and DES simulations. The computed difference between the refined mesh results at 2x and 4x the wake resolution for the DES simulations and the experimental data is presented in Fig. 14. The near-wall body-conforming grids are unaltered. The r.m.s. difference in velocity magnitude computed over all experimental points is tabulated for both the RANS and DES simulations in Table 2. The average difference is between 5 and 10% of the freestream velocity magnitude, with the DES results slightly lower. Mesh refinement does not significantly reduce the difference between the computed results and the PIV measurements. This can be due to errors in the CFD predictions, *e.g.* delayed prediction of the primary flow separation on the capsule forebody which is roughly independent of wake resolution, or simply that the uncertainty in the PIV measurements are of the same order as the differences being computed.

4 Numerical Scheme

The current work investigates two choices for numerical scheme: central differencing of the convective and acoustic terms, and the upwind HLLC flux in a Monotonic Upstream-Centered Scheme for Conservation Laws (MUSCL) implementation. The upwind flux is often preferred for capsule aerodynamic database development due to the improved performance (robustness, shock-capturing) for high-speed flows, and the desire to maintain a single scheme for all database computations, as in [18]. Further, when modeling reaction-

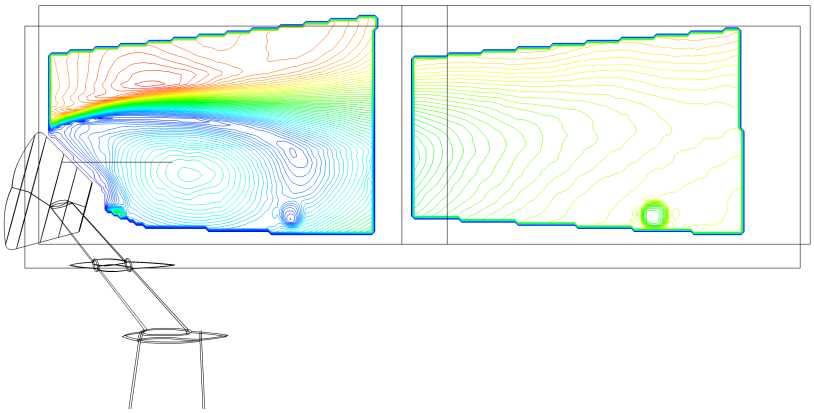

(a) PIV

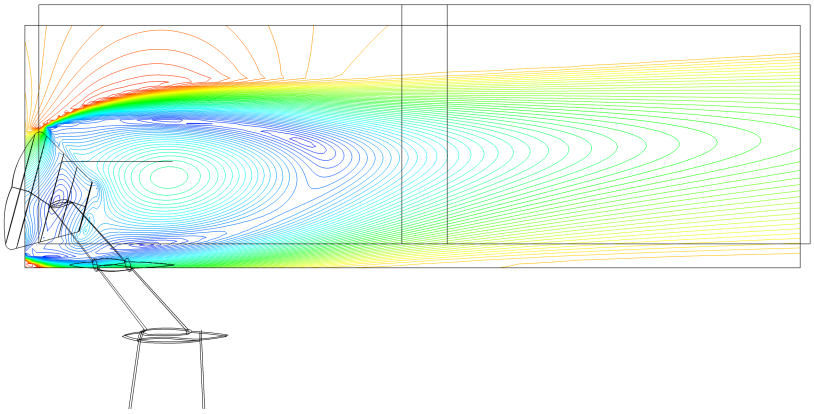

(b) RANS

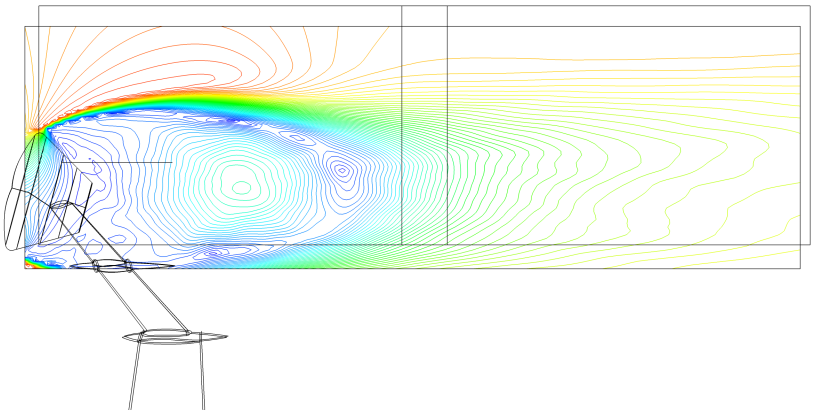

(c) DES

Figure 12: Measured and computed velocity magnitude in the wake. $M_\infty = 0.5$, $\alpha = 166°$, $Re_D = 8.7$M. Experimental data taken from [9].

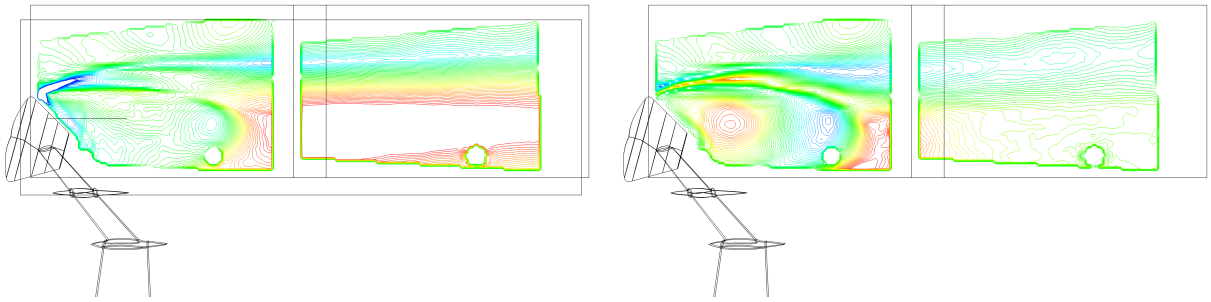

(a) RANS **(b)** DES

Figure 13: Difference in the wake velocity magnitude between simulation and PIV measurement (PIV-CFD), scaled by the freestream velocity magnitude. The limits of the difference are $\pm 0.25 M_\infty$. Green contours represent zero. $M_\infty = 0.5$, $\alpha = 166°$, $Re_D = 8.7$M.

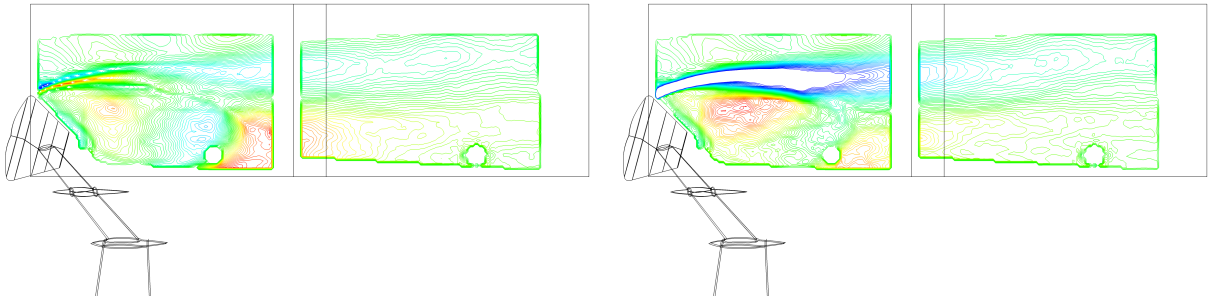

(a) 2x **(b)** 4x

Figure 14: Difference in the wake velocity magnitude between simulation and PIV measurement (PIV-CFD) for the refined DES simulations, scaled by the freestream velocity magnitude. The limits of the difference are $\pm 0.25 M_\infty$. Green contours represent zero. $M_\infty = 0.5$, $\alpha = 166°$, $Re_D = 8.7$M.

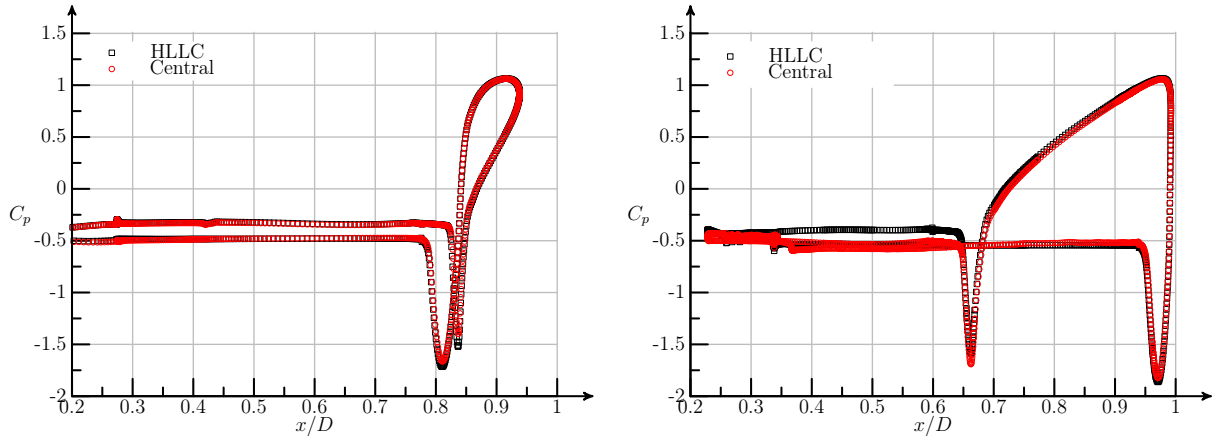

(a) Baseline **(b)** Adapted

Figure 15: Surface pressure distribution down the pitch plane of a generic isolated capsule configuration. $M_\infty = 0.5$, $\alpha = 160°$, $Re_D = 24$M.

control system (RCS) jets either the chemistry of the plumes or passive-scalar convection of thermodynamic quantities to model the chemistry is included. In these cases, the upwind schemes have proven necessary for robustness[18], and hence to achieve consistent increments in the subsonic regime when modeling RCS, an upwind scheme may be necessary. The central-differencing schemes are often preferred for low-speed separated flows due to their lower numerical dissipation, especially when higher-order schemes are utilized, and due to the lower computational cost.

The two schemes are compared on the isolated capsule from the previous experimental configuration for simplicity. The computed pressure distributions down the pitch plane of the capsule are presented in Fig. 15*. Both simulations use the SST RANS turbulence model. Fig. 15a uses the baseline resolution from Fig. 3 (30M grid points in the capsule region), while Fig. 15b is adapted and uses roughly 100M grid points in the capsule region. The stagnation point on the heatshield produces the peak pressure, and the suction near the primary boundary layer separation produces the lowest pressure. The largest differences are seen in the aft-body region of the adapted case, though the differences overall are relatively minor. Both schemes are consistent, and are expected to converge to the same answer with further mesh refinement. In situations where robustness is imperative, the HLLC is preferred, but the central differencing can be significantly lower cost (5x-10x), which is important for unsteady DES simulations.

*The geometry in Fig. 15a is aligned with the x coordinate, while Fig. 15b is rotated by the angle of attack, hence the difference in pressure distribution along the x axis.

5 Rotation and Curvature Correction

The attached flow on the capsule forebody curves around the constant radius of the heatshield. It is well documented that streamline curvature in the plane of the mean shear has a strong effect on the turbulent Reynolds stresses. To account for these effects, rotation and curvature corrections for one- and two-equation turbulence models are common. Here we examine the correction proposed by Spalart and Shur[19]. Unfortunately, this correction adversely effects the flow predictions in the bluff-body wake. The approach used here is to apply the rotation and curvature correction in a zonal manner, *i.e.* only in the boundary layer region near the wall. This is easily accomplished in an overset approach by splitting the body-conforming grids at a prescribed location. The result on the computed pressure distribution using the SST RANS turbulence model is presented in Fig. 16. The rotation and curvature correction diminishes the strength of the suction peak due to the primary separation, by reducing the turbulent eddy viscosity and causing the boundary layer to separate earlier. This is consistent with available experimental evidence for similar configurations, and the results of Fig. 11, which shows the baseline model tends to overpredict the suction in the separation region.

6 *In Toto*

The current work outlines several issues in numerical methods and physical modelling related to the accuracy of aerodynamic predictions for capsule configurations. The validity of remedying these issues is established by comparison with recent high-Reynolds-number experimental results. The results are summarized by applying them to the same configuration outlined in the Introduction in Fig. 3. The use of wall roughness modeling, the SST turbulence model with rotation and curvature corrections and DES model, and low-dissipation central differencing schemes are combined with recent enhancements for near-wall and off-body mesh adaptation in OVERFLOW. While a formal grid convergence study is not presented for the DES simulations, it is acknowledged that the baseline results presented in Fig. 3 were a practical necessity and are not considered sufficient to resolve all scales of the complex flowfield. To improve upon this approach, while still restricting the computational cost to a practical level, mesh adaptation is utilized.

Figure 17 presents feature-based mesh adaptation around the capsule at three increasing angles of attack. The solver automatically adapts to the separated shear-layer and aft-body region resulting in a mesh in the capsule region of approximately 100M points. The

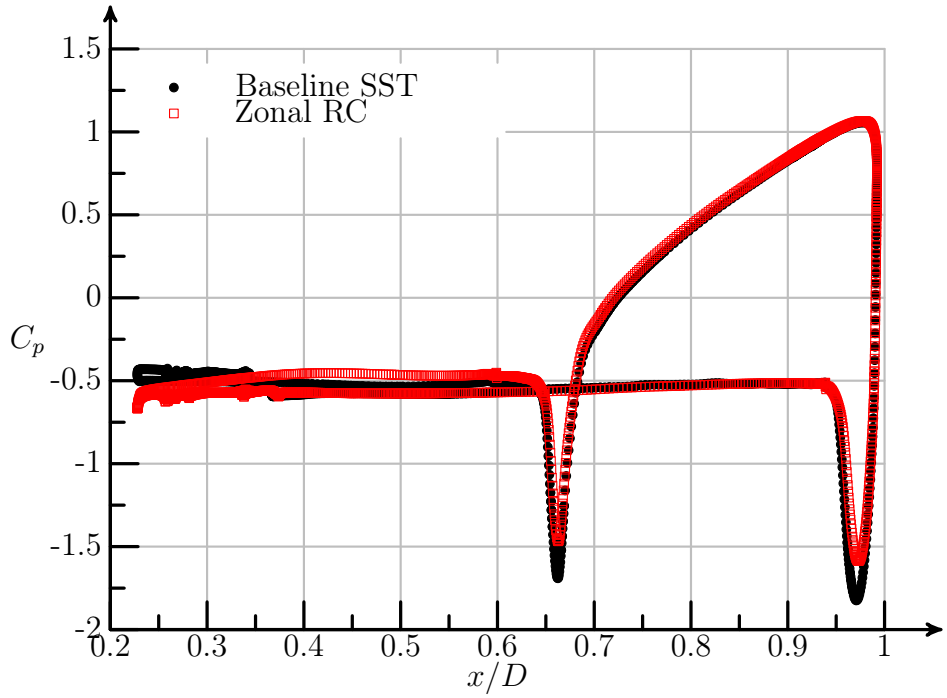

Figure 16: Surface pressure distribution down the pitch plane of a generic isolated capsule configuration. $M_\infty = 0.5$, $\alpha = 160°$, $Re_D = 24$M.

resulting integrated loads, shown in Fig. 18, are averaged over a statistically stationary state of the DES simulations which covers roughly 1 second. While there is still room for improvement, the CFD simulations are now largely within the experimental uncertainty. The sigmoidal shape of the pitching moment curve is captured, and the normal force is well predicted at all angles of attack. The drag predictions are now consistent and closer to the experimental data. These improvements do come at a cost of greater resolution, however in this case this is offset by the reduced computational cost from central differencing. The computed configuration does not include all of the geometric features on the heatshield of the experimental configuration, which does account for some of the observed increments in drag and pitching moment. Further, both the experiment and CFD simulations are corrected using the local pressure around the base of the sting, which may be part of the discrepancies.

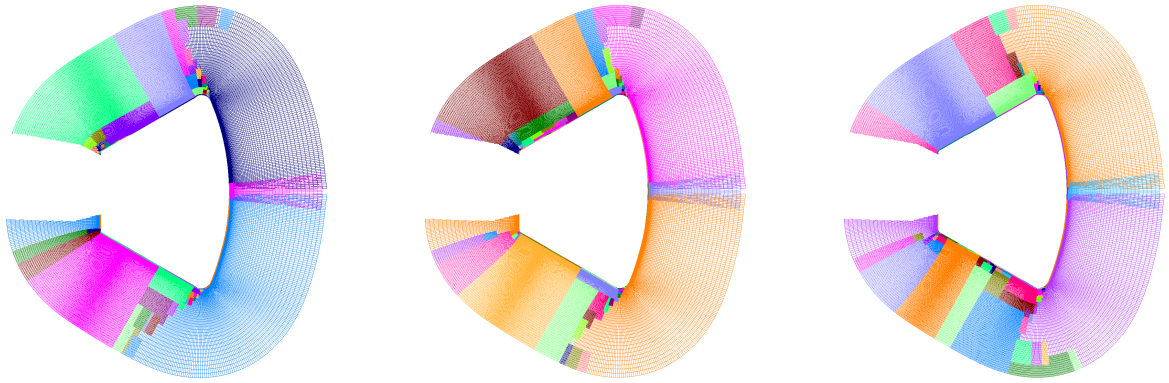

(a) $\alpha = 160°$ **(b)** $\alpha = 172°$ **(c)** $\alpha = 184°$

Figure 17: Adapted body-conforming overset grids in the lateral plane of symmetry.

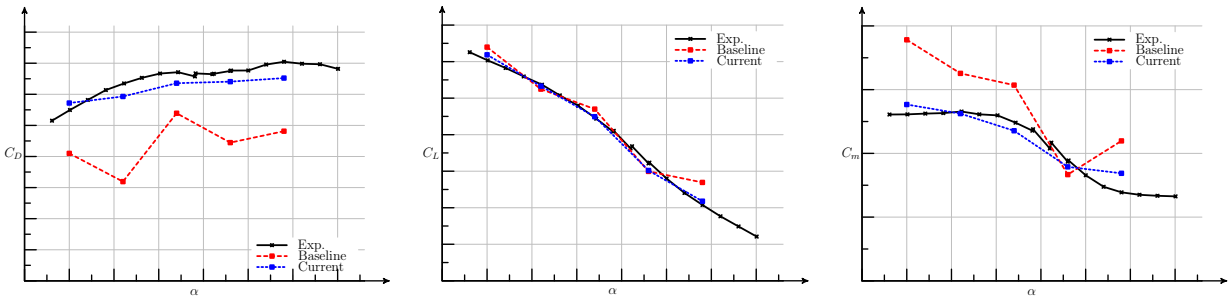

(a) Drag **(b)** Lift **(c)** Pitching Moment

Figure 18: Computed and experimental integrated loads for an Orion capsule geometry using methods described in the current work. $M_\infty = 0.5$, $Re_D = 24$M.

7 Summary

Recent high-Reynolds-number wind tunnel data for capsule aerodynamics has removed much of the uncertainty associated with previous experimental validation datasets. The state of the boundary layer on the capsule heatshield is well characterized and correctly accounts for the surface roughness expected after ablation for the Orion configuration. Using this data, several aspects of the numerical predictions of CFD methods were investigated, and the results indicate that methods which improve the accuracy of the physical modeling - wall roughness, DES unsteady wake, streamline curvature - do produce improvements in the predictive capability of the simulations. Combined with improved mesh resolution and adaptive methods, computations in the subsonic regime using these approaches demonstrate noticeable improvements.

Acknowledgments

Dr. Stuart Rogers of NASA Ames Research Center and Darby Vicker of NASA Johnson Space Center provided the grid systems for the experimental capsule configurations.

References

[1] Fujimoto, K., Fujii, K., and Tsuboi, N., "CFD Prediction of the Aerodynamic Characteristics of Capsule-Like Configurations for the Future SSTO Development," AIAA Paper 2003-912, 2003.

[2] Chaderjian, N.M. and Olsen, M.E, "Grid Resolution and Turbulence Model Effects on Space Capsule Navier-Stokes Simulations," AIAA Paper 2007-4562, June 2007.

[3] Stremel, P.M., McMullen, M.S., and Garcia, J.A., "Computational Aerodynamic Simulations of the Orion Crew Module," AIAA Paper 2011-3503, 2011.

[4] Schwing, A. and Candler, G., "Validation of DES for Capsule Aerodynamics using 05-CA Wind Tunnel Test Data," AIAA Paper 2013-0644, 2013.

[5] Moseley, Jr., W.C., Graham, R.E., and Hughes, J.E., "Aerodynamic Stability Characteristics of the Apollo Command Module," NASA TN D-4688, August 1968.

[6] Bell, J.H., "Test 5-CA Final Report," CEV Aerosciences Project Report EG-CEV-06-19, 2006.

[7] Murphy, K.J., Bibb, K.L., Brauckmann, G.J., Rhode, M.N., Owens, B., Chan, D.T., Walker, E.L., Bell, J.H., and Wilson, T.M., "Orion Crew Module Aerodynamic Testing," AIAA Paper 2011-3502, 2011.

[8] Brauckmann, G., Chan, D., and Walker, E., "Final Report for Test 89-CA: High-Reynolds Number Test of the Orion Crew Module in the NASA LaRC National Transonic Facility," Tech. Rep. EG-CAP-12-65, MPCV Aerosciences, 2012.

[9] Ross, J.C., Heineck, J.T., Halcomb, N., Yamauchi, G.K., Garbeff, T., Burnside, N.T., Kushner, L.K., and Sellers, M., "Comprehensive Study of the Flow Around a Simplified Orion Capsule Model," AIAA Paper 2013-2815, 2013.

[10] Nichols, R.H., Tramel, R.W., and Buning, P.G., "Solver and Turbulence Model Upgrades to OVERFLOW 2 for Unsteady and High-Speed Applications," AIAA Paper 2006-2824, 2006.

[11] Menter, F.R., "Two-Equation Eddy-Viscosity Turbulence Models for Engineering Applications," *AIAA Journal*, vol. 32, no. 8, pp. 1598–1605, 1994.

[12] Nikaido, B.E., Murman, S.M., and Garcia, J.A., "OpenFOAM Simulations of Compressible High Reynolds Number External Aerodynamics," accepted for AIAA SciTech 2015.

[13] Buning, P.G. and Pulliam, T.H., "Cartesian Off-body Grid Adaptation for Viscous Time-Accurate Flow Simulation," AIAA Paper 2011-3693, 2011.

[14] Buning, P.G. and Pulliam, T.H., "Initial Implementation of Near-Body Grid Adaptation in OVERFLOW," in *11th Symposium on Overset Composite Grid and Solution Technology*, 2012.

[15] Knopp, T., Eisfeld, B., and Calvo, J.B., "A new extension for $k-\omega$ turbulence models to account for wall roughness," *International Journal of Heat and Fluid Flow*, vol. 30, pp. 54–65, 2009.

[16] Spalart, P.R. and Allmaras, S.R., "A one-equation turbulence model for aerodynamics flows," *La Recherche Aérospatiale*, vol. 1, pp. 5–21, 1994.

[17] Wilcox, D.C., "Formulation of the k-ω Turbulence Model Revisited," AIAA Paper 2007-1408, January 2007.

[18] Childs, R.E., Garcia, J.A., Melton, J.E., Rogers, S.E., Shestopalov, A.J., and Vicker, D.J., "Overflow Simulation Guidelines for Orion Launch Abort Vehicle Aerodynamic Analyses," AIAA Paper 2011-3163, June 2011.

[19] Spalart, P.R. and Shur, M.L., "On the Sensitization of Turbulence Models to Rotation and Curvature," *Aerospace Science and Technology*, vol. 1, no. 5, 1997.